Int J Appl Earth Obs Geoinformation 78 (2019) 202–214

Contents lists available at ScienceDirect

Int J Appl Earth Obs Geoinformation

journal homepage: www.elsevier.com/locate/jag

Mapping land cover change in northern Brazil with limited training data

Merry Crowson[a,*], Ron Hagensieker[a], Björn Waske[b]

[a] Freie Universität Berlin, Institute of Geographical Sciences, Malteserstr. 74-100, 12249 Berlin, Germany
[b] Remote Sensing Group, Institute of Computer Science, Osnabrück University, Wachsbleiche 27, 49090 Osnabrück, Germany

ARTICLE INFO

Keywords:
Import vector machines (IVM)
Change detection
Probabilistic classifier
Land cover classification

ABSTRACT

Deforestation in the Amazon has important implications for biodiversity and climate change. However, land cover monitoring in this tropical forest is a challenge because it covers such a large area and the land cover change often occurs quickly, and sometimes cyclically. Here we adapt a method which eliminates the need to collect new training data samples for each update of an existing land cover map. We use the state-of-the-art probabilistic classifier Import Vector Machines and Landsat 8 Operational Land Imager (OLI) scenes of the area surrounding Novo Progresso, northern Brazil, to create an initial land cover map for 2013 with associated classification probabilities. We then conduct spectral change detection between 2013 and 2015 using a pair of Landsat images in order to identify the areas where land cover has changed between the two dates, and then reclassify these areas using a supervised classification algorithm, using pixels from the unchanged areas of the map as training data. In this study, we use the pixels with the highest classification probabilities to train the classifier for 2015 and compare the results to those obtained when pixels are chosen randomly. The use of probabilities in the selection of training samples improves the results compared to a random selection, with the highest overall accuracy achieved when 250 training samples with high probabilities are used. For training sample sizes greater than 1000, the differences in overall accuracy between the two approaches to training sample selection are reduced. The final updated 2015 map has an overall accuracy of 80.1%, compared to an overall accuracy of 82.5% for the 2013 map. The results show that this probabilistic method has potential to efficiently map the dynamic land cover change in the Amazon with limited training data, although some challenges remain.

1. Introduction

The Amazon rainforest spreads over 550 million hectares (Kintisch, 2015) and is the planet's largest tropical rainforest. It covers parts of nine countries, but the largest proportion is in Brazil. This tropical ecosystem is threatened by large scale deforestation, forest degradation and agricultural expansion (Lapola et al., 2014). For example, in 2016 a total area of 7989 km^2 was deforested in the Legal Amazon, a 29% increase on the 6207 km^2 cleared in 2015 (INPE, 2016).

Deforestation in the Brazilian Amazon has received a lot of attention since the 1980s, including concerns over the loss of biological diversity (Hooper et al., 2012) and the connection between deforestation in the north and the prolonged drought of 2014 and 2015 in southern Brazil (Nobre, 2014). However, it is very likely that the main drivers of land transformation and forest loss, namely cattle ranching, soy farming and the timber trade, are set to continue into the future (Rufin et al., 2015).

If environmental protection is to be factored into future cost-benefits analysis regarding the Amazon, monitoring land cover is essential. Land cover information promotes better informed land use planning and decision making for the Amazon region (Almeida et al., 2016). In addition, the important role of the Amazon in global (Betts et al., 2004) and regional climate (Swann et al., 2015), including its role as a carbon sink within the carbon cycle (Pan et al., 2011), makes a better understanding and quantification of land cover essential input into climate change models that attempt to predict future change in the system (Werth and Avissar, 2002). However, monitoring land cover change in this tropical ecosystem is challenging because of the size of the ecosystem, and also because much of the land cover change occurs rapidly, through clear cutting and burning, and cyclically (Hagensieker et al., 2017). Müller et al. (2016b) analyse the spatial-temporal patterns of regrowth of secondary vegetation after deforestation in southern Amazonia. They show that regrowth often occurred cyclically, with most of the regrowth occurring within the first three years after primary forest has been cleared, and that the secondary vegetation is then often re-cleared to increase productivity.

In this context, remote sensing is in a unique position to contribute,

* Corresponding author. Present address: Institute of Zoology, Zoological Society of London, Outer Circle, Regent's Park, London NW1 4RY, United Kingdom.
E-mail address: merry.crowson@ioz.ac.uk (M. Crowson).

https://doi.org/10.1016/j.jag.2018.10.004
Received 4 July 2018; Received in revised form 5 October 2018; Accepted 7 October 2018
Available online 22 February 2019
0303-2434/

as it offers the possibility of mapping land cover over large areas at a high temporal resolution. During the last decade the general development in land cover mapping using remote sensing images was driven by a shift to more flexible machine-learning algorithms. Methods such as Support Vector Machines and Random Forest have emerged over the past decade and are widely used to classify various remote sensing data (Waske and van der Linden, 2008; Waske et al., 2010; Mountrakis et al., 2010; Belgiu and Drăguţ, 2016). Despite these developments, one of the major challenges remains how to automate land cover mapping as much as possible, in order to reduce both the time and cost of mapping projects. In particular, a large effort is required to collect training samples for supervised classification (Müller et al., 2016a). This is particularly important as a sufficient number of training samples ensures that adequate training samples are included during classification (Foody and Mathur, 2004).

In the United States, the Multi-Resolution Land Characteristics Consortium have developed their own response to the aforementioned challenge in order to provide data on land cover and land cover change for the conterminous USA and Puerto Rico at 30 m resolution and in 5-year cycles, called the National Land Cover Database (NLCD) (Fry et al., 2011). As described in Xian et al. (2009), they apply spectral change detection to a pair of Landsat images in order to identify the areas where land cover has changed between the two dates, and then reclassify these areas using a supervised classification algorithm, using pixels from the unchanged areas of the map as training data. We refer to this two-step method as the spectral change detection-supervised classification (SCD-SC) method, as a generalised version, because the details of the method they used in this two-step process varied between editions of the NLCD (Xian et al., 2009; Fry et al., 2011; Homer et al., 2015). However, in these studies, the training pixels for the supervised classification were taken randomly from the area detected as unchanged by the change detection.

In this paper, we propose an extension of the SCD-SC method to map land cover change in the Brazilian Amazon. The classification is based on the probabilistic classifier Import Vector Machines (IVM) (Zhu and Hastie, 2005). IVM is a supervised, non-parametric classifier which has been shown to have reliable probabilistic outputs (Roscher et al., 2012a, b). The probabilities associated with the classification result, here called classification probabilities, represent the confidence in the class label and are used as criteria for training data selection.

To this end, the two main objectives of this study are: (1) explore the potential of using classification probabilities as criteria for training data selection within the SCD-SC method and (2) assess the suitability of the modified SCD-SC method for use in a tropical forest system.

2. Study site and data

2.1. Study area

The study site is a 170 km by 178 km area, corresponding to a single Landsat footprint, located in the Municipality of Novo Progresso, within the Province of Pará, Brazil (Fig. 1). It is intersected by the BR-163 highway and is centred around the city of Novo Progresso.

The land cover in the area is dominated by dense evergreen forest (DNPM, 1983) and the deforested areas are predominantly used for extensive and traditional cattle farming (Jakimow et al., 2018). The BR-163 highway was built in the 1970s and connects the region to globalized markets (Coy and Klingler, 2011). The urban area of Novo Progresso lies towards the centre of the study site on the BR-163 highway. There are some areas of hilly terrain close to Novo Progresso where tree density is lower due to rock outcrops (Müller et al., 2016a).

The regional climate is characterised by a wet and a dry season, with the dry season running from June to September (Müller et al., 2016b). The seasonality of rainfall influences land cover change, with large scale deforestation occurring during the dry season, as transport is easier along the logging and transport roads when rainfall is lower

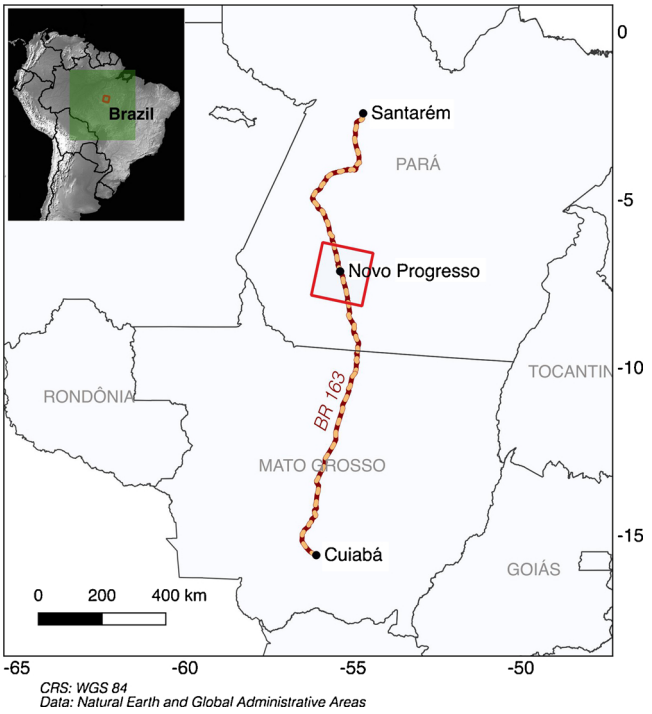

Fig. 1. Overview map of the study site, showing a section of the BR-163 highway and the extent of the study site (red box). (For interpretation of the references to colour in this figure legend, the reader is referred to the web version of this article.)

(Aragão et al., 2008). However, on land that has been converted to pasture, burning and resowing of forage grasses often takes place towards the beginning of the wet season to minimise regrowth of secondary vegetation and maximise the productivity of the land (Asner et al., 2004).

2.2. Remote sensing data

Four Operational Land Imager (OLI)/Landsat 8 provisional Surface Reflectance Products were used throughout this study (USGS, 2016) (Fig. 2), including bands 2–7 in their native resolution of 30 m. All the Landsat scenes are from WRS path 227 and row 065, but were clipped slightly to a standard size to ensure that they all have the same extent. The cloud and cloud shadow mask included in the product (CFmask) was used to mask cloud cover as necessary. The proposed change detection method requires a two-date pair of scenes obtained over the same geographical area. In order to detect land cover change between years, it is usually recommended that scenes be chosen from the same season to reduce the impact of seasonal and phenological variability, as areas that change due to seasonal variability may be confused with those undergoing land cover change (Xian et al., 2009; Lu et al., 2004). Landsat scenes from the 24th August 2013, corresponding to the day of year (DOY) 236, and 14th August 2015 (DOY 226) were chosen as their DOY are only 10 days apart, whilst having less than 10% cloud cover (Fig. 2; Table 1).

For the land cover classification, two scenes were used for each year. Using multitemporal images as inputs has been reported to improve classification accuracy (e.g. Zhu et al., 2012), particularly for vegetation, because of the phenological characteristics of different vegetation types. For example, in this study, pasture and secondary vegetation are likely to present seasonal changes due to changes in water availability, whilst forest will not experience such marked variation. Unfortunately, because of very high cloud cover in the study area during the wet season (October–May), only images from within the dry season could be used in this study. The second image for each year was

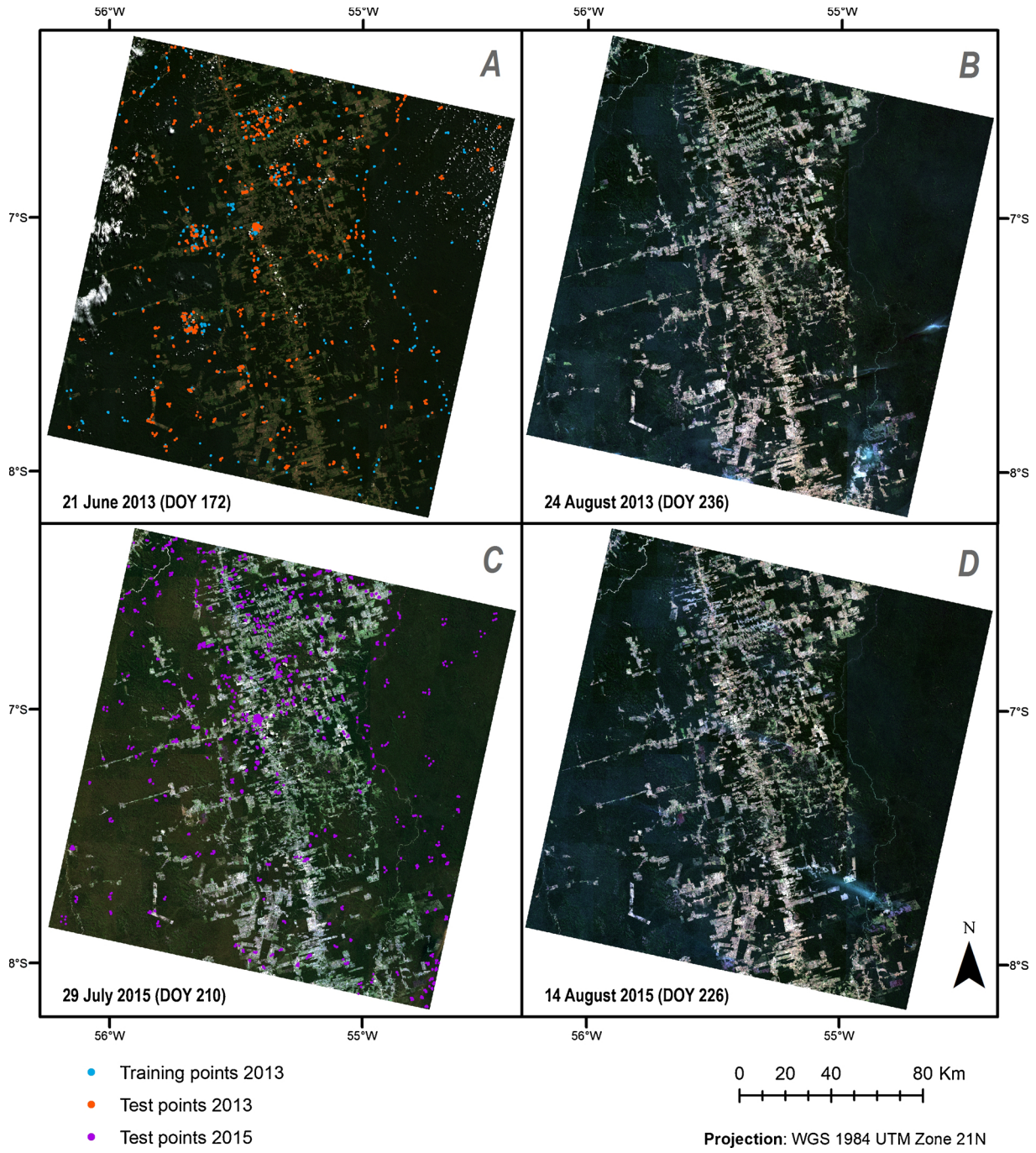

Fig. 2. True colour Landsat 8 scenes used in this study. Scenes B and D were used for change detection purposes, A and B for the 2013 land cover classification, and C and D for the 2015 land cover classification. The percentage cloud cover for each scene is: A 1.13% B 0.04%, C 0.03% and D 0.09%. Additionally, the training and test data used for the classifications are displayed on maps A and C.

Table 1
Summary of the scenes used in this study and their properties. The change detection used the scenes from the 24th of August 2013 and the 14th of August 2015. Two scenes from each year were used in the classifications. Bands 2–7 were included throughout the analysis.

Satellite	Sensor	Product	Date	WRS path/row	Resolution	Cloud cover
Landsat 8	Operational Land Imager (OLI)	Surface Reflectance (SR)	21 June 2013	227/065	30 m	1.13%
Landsat 8	OLI	SR	24 August 2013	227/065	30 m	0.04%
Landsat 8	OLI	SR	29 July 2015	227/065	30 m	0.03%
Landsat 8	OLI	SR	14 August 2015	227/065	30 m	0.09%

Table 2
Description of the classes used in this study.

Class	Description
Forest	Primary dense evergreen forest (DNPM, 1983)
Pasture	Pasture in productive process with a predominance of herbaceous species or at an initial stage of the secondary succession (Galvão et al., 2009), containing shrubs and early successional vegetation.
Secondary Vegetation	Areas with perennial bushes, palms and tree species which colonize forest gaps and overgrow forage grasses on pasture areas (Müller et al., 2016b). Includes areas at an intermediate and advanced stage of secondary succession which were once clear-cut for forestry or agriculture (Galvão et al., 2009).
Urban	Area where the dominant land cover is man-made, impermeable surfaces, such as buildings and roads.
Water	Rivers, lakes and ponds.

chosen to be temporally as far as possible from the first, whilst minimising cloud cover. The second two images are for 21st of June (DOY 172) 2013 and 29th of July (DOY 210) 2015. Our preliminary classifications results showed an increase in accuracy when two scenes were used for each year, suggesting that the classes respond differently to the decrease in water availability as the dry season progresses.

2.3. Reference data and definition of land cover classes

The following classes were used in this study: forest, pasture, secondary vegetation, urban and water. These classes are described in Table 2 and include the main land cover types in the study area (Almeida et al., 2016), although a few simplifications were necessary. The pasture class includes both shrubby pasture and grassy pasture (Almeida et al., 2016; Rufin et al., 2015; Hagensieker et al., 2017). Both types of pasture are generally used for cattle ranching in the region, with grassy pasture being more intensely managed and characterised by a land cover of grass species. Shrubby pasture, on the other hand, is in an initial stage of secondary succession (Galvão et al., 2009), with a higher percentage of shrubby vegetation (Almeida et al., 2016).

Secondary vegetation is a class considered in various studies (Almeida et al., 2016; Hagensieker et al., 2017; Müller et al., 2016b) in order to distinguish between highly diverse primary forest and forest that has recently grown back after management ceased. This allows a distinction to be made between deforestation as a removal of primary forest and agricultural management practices that cyclically remove vegetation cover with less ecological value. Secondary vegetation is dominated by intermediate to advanced stages of succession (Galvão et al., 2009).

We did not include a class for annual crops in our analysis because it only covers a very small proportion of our study area according to the TerraClass datasets (Almeida et al., 2016). Although the TerraClass dataset does map some small areas in our study area as degraded pasture, containing at least 50% bare soil, our initial efforts to include a separate class for bare soil did not provide good results. Thus, in this study the classes urban and pasture are both likely to include some bare soil, often as mixed pixels with other land cover types such as impermeable surfaces or pasture.

Reference data for the study region was produced based on visual examination of Landsat scenes, Google Earth and, when available, Rapid Eye images. In addition, PRODES and TerraClass land cover data were available for the study site and used to identify areas of secondary vegetation. PRODES (Programa de Cálculo do Desflorestamento da Amazônia) records annual increments of deforestation in the Legal Amazon (August–July), with a minimum mapping unit of 6.25 ha (INPE, 2016). TerraClass builds on PRODES by creating a detailed map of land use and land cover (LULC) in the deforested areas of the Brazilian Legal Amazon (Almeida et al., 2016). Secondary vegetation was also identified by checking Landsat images as far back as 1988 and identifying areas of pasture in an earlier Landsat image that are at an intermediate to advanced stage of secondary succession 5+ years later (Galvão et al., 2009).

3. Methods

3.1. General concept

The proposed SCD-SC method uses IVM for the supervised classifications. IVM have been successfully used for diverse remote sensing applications and their performance has been tested and evaluated with regards to classifying hyperspectral and multisensor remote sensing data (Hagensieker et al., 2017; Suess et al., 2014; Roscher et al., 2012b; Braun et al., 2012). The results show that IVM perform comparably well to, or slightly better than the widely-used Support Vector Machine (SVM) classifier in terms of overall accuracy, and can be computationally more efficient than SVM (Rosentreter et al., 2017). Moreover, IVM directly provide probabilities of class memberships, which can be more accurate than the (pseudo)probabilities provided by SVM (Roscher et al., 2012a,b; Rosentreter et al., 2017).

The spectral change detection step uses a spectral index called Relative Change Vector Maximum (RCVMAX) (Fry et al., 2011), but otherwise follows the method from Xian et al., 2009, briefly described in Section 3.2.

The workflow for this study is as follows (see Fig. 3): (i) Classification for 2013, creating a land cover map and a map of probabilities to serve as a starting point for the SCD-SC method, (ii) spectral change detection between a 2013 scene and a 2015 scene, in order to distinguish between areas of change and no-change, (iii) classification for 2015, using pixels from the area detected as unchanged in step (ii) to train the classifier and re-classify only the areas detected as changed. This third step was carried out repeatedly with different amounts of training data, following two approaches: a) training data taken randomly from the unchanged areas and b) training data chosen from the unchanged area with the top classification probabilities in each class from the 2013 classification.

Finally, an accuracy assessment was performed for all classifications in order to compare the different maps. The confusion matrices were used to derive overall accuracy, producer's and user's accuracies, and the kappa coefficient of agreement.

3.2. Land cover classification 2013

An initial land cover map was produced by classifying two scenes from 2013. The training sample included just under 1000 points, with approximately 200 taken from each class. The independent test data set comprised 1850 samples in total. The IVM classifier was used for the classification in the Matlab environment (Roscher, 2014). This implementation of the IVM algorithm uses grid search to optimise the two main parameters for the model, λ and σ, which are analogous to Support Vector Machines' cost and kernel parameters, respectively. For this a 5-fold cross validation was used. The parameter σ is the kernel parameter, which indexes the radial kernel and thus maps the features into higher dimensional space. The regularization parameter λ balances the fitting of the model (Roscher et al., 2012b). The output of the IVM classification for each pixel is the probability of class membership for each class. The class with the highest probability is taken as the final class label.

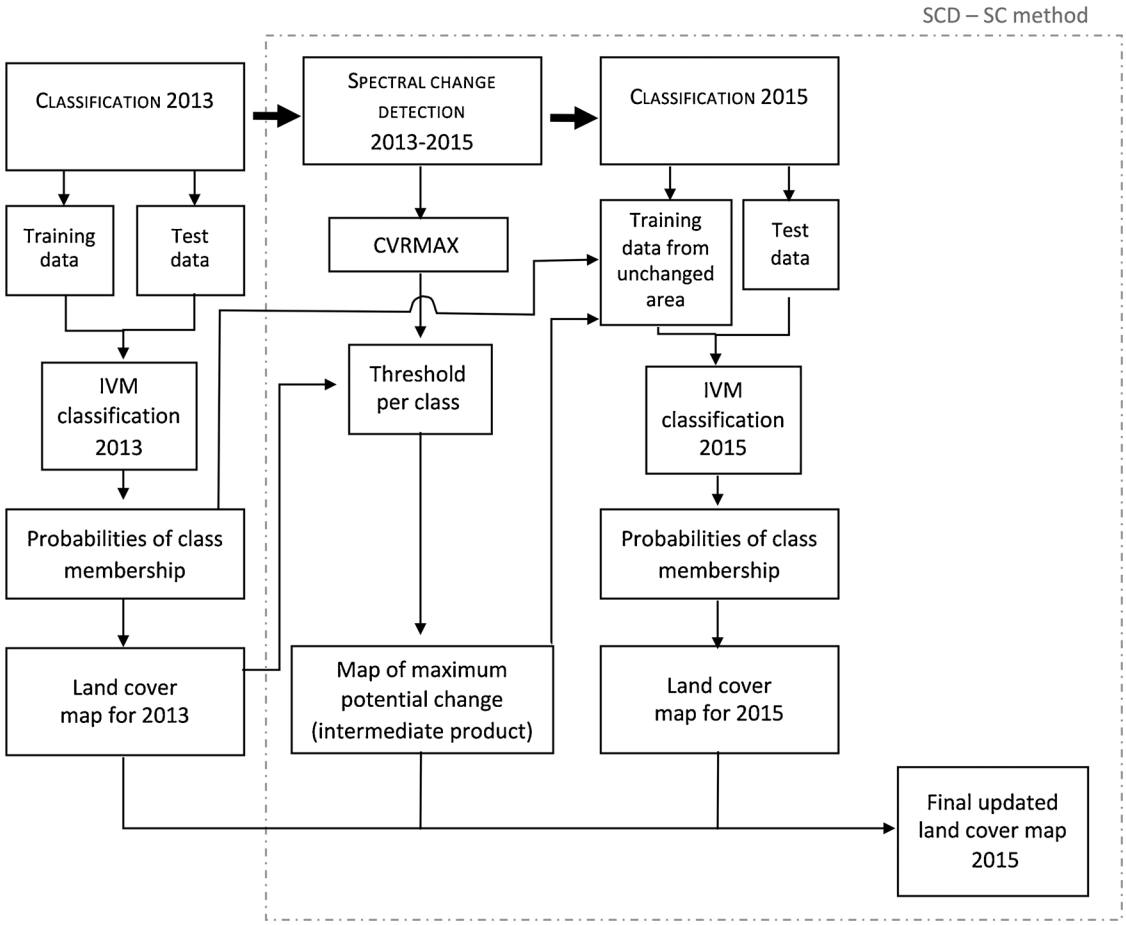

Fig. 3. Generalized workflow for this study. The large dashed box surrounds the steps that make up the Spectral Change Detection –Supervised Classification method.

3.3. Spectral change detection (2013–2015)

Identifying areas of land cover change between the Landsat images from 2013 and 2015 is important to be able to successfully update the 2013 land cover map to 2015. Accurate detection of changed areas for each class ensures that these pixels do not go on to form part of the training pool for the 2015 classification and ensures that they are re-classified. With this in mind, the objective was to minimise omission error for the change area, as described in Fry et al. (2009), whilst keeping a reasonably large area to sample for unchanged pixels and avoid reclassification of an unnecessarily large area. Thus minimising omission error for the change area is the main objective, and reducing commissioning error for the change area a secondary concern. This approach to spectral change detection results in a map of "maximum potential change" (Jin et al., 2013), in which the amount of change can be assumed to be overestimated and thus represents a theoretical maximum amount.

We use the RCVMAX change detection method (Xian et al., 2009; Fry et al., 2011). The main steps are: pre-processing, image differencing and setting a threshold for bi-temporal change detection. Finally, the accuracy of the binary change map is assessed. In terms of pre-processing, the Landsat scenes from the 24th of August (DOY 236) 2013 and 14th of August (DOY 226) 2015 were masked with the clouds from both scenes.

The RCVMAX was calculated for each pixel in the R environment, following Jin et al. (2013):

$$\mathrm{RCVMAX} = \sum_i [(B_{1i} - B_{2i})/\max(B_{1i}, B_{2i})^2]$$

where $B_{1i}(i = 2...7)$ is the i th band of the 2013 Landsat 8 image, $B_{2i}(i = 2...7)$ means the i th band of the 2015 Landsat 8 image, and $\max(B_{1i}, B_{2i})$ denotes the maximum value of B_{1i} and B_{2i}.

RCVMAX can quantify the magnitude of relative change and shows a general change pattern. A greater RCVMAX indicates a higher possibility of change (Fry et al., 2011). The RCVMAX was chosen because by taking into account the maximum value of each band and describing pixel values relative to this, it is expected to better account for changes in illumination between the scenes.

The adjustable parameters to determine the threshold for bi-temporal change detection, that is, how much spectral change can occur before a pixel is said to have changed class, was set per class. This is because some land cover types have more spectral variability, both seasonally and inter-annually (Huang et al., 2010). The condition is defined as

$$RCVMAX_j(x, y) = \begin{cases} change\ if\ |RCVMAX_j(x, y)| \geq |\overline{RCVMAX_j}| + a_j\sigma_j \\ no - change\ if\ |RCVMAX_j(x, y)| < |\overline{RCVMAX_j}| + a_j\sigma_j \end{cases}$$

where j represents a land cover class, $|RCVMAX_j|$ is the mean of the RCVMAX for the land cover type j, σ_j is the standard deviation of the $RCVMAX_j$, and a_j is an adjustable parameter.

Morisette and Khorram (2000) demonstrated that the optimal range of a_j is from 0.0 to 1.5 for a single threshold, so this range was tested for each class in steps of 0.25. The choice of the adjustable parameter a_j was based solely on visual inspection of the resulting change map. In each case the resulting change map was compared with the two Landsat 8 scenes and considered in relation to existing information on how much land change is likely to have occurred in each land cover type.

As the final, updated land cover map for 2015 relies on adequate

change detection, we assess the accuracy of the binary change map. As described earlier in this section, the thresholds were set to minimise the error of omission for the change area, because the priority is to avoid pixels falsely identified as unchanged entering the training pool for 2015.

Samples were taken from two strata, “change” and “no-change”. A total of 95 points were taken randomly from the area identified as “change” and 218 points from “no-change”. We took most of the samples randomly from the “no-change strata”, but we also targeted areas more likely to change (Congalton and Green, 2009), including areas close to “change” and areas with the land class label forest in 2013. The spatial distribution of the test points can be viewed in the results section on the binary change map (Fig. 5). Test points were labelled visually as “change” or “no-change” based on the Landsat images used for change detection. TerraClass data was used to distinguish secondary vegetation from primary forest.

3.4. Land cover classification 2015

The training data was taken from the areas mapped as unchanged between 2013 and 2015, following the method described in 3.3. Training data was chosen within the unchanged area in two ways: (i) randomly from within the unchanged area, and (ii) pixels with the highest classification probabilities in each class. For each of the two approaches, the total number of training data n was also varied, with $n \in \{25,75,125,250,1000,3000,6000\}$. In each case an equal number of pixels was taken per class. Each training sample set was used to train a separate IVM classifier, while the same test data set was used in each case (Table 3). The test points were taken throughout the whole scene (Fig. 2).

Because the training samples were randomly selected from each class in approach (i), the result of the classification can be expected to vary with the sample selection. Thus the 2015 IVM classification was run 10 times for each sample set size (i.e. 25, 75, …, 6000). In approach (ii) (selection using classification probabilities) the same training set was used in each run. Finally, the results were averaged and the mean accuracy and standard deviation reported in each case.

McNemar’s test for paired-sample nominal scale data (Agresti, 2002) was used to assess if a statistically significant difference exists between the classifications with the highest overall accuracy from the two approaches to training sample selection. This test is suitable to assess the performance of classifications that use the same test samples (Foody, 2004).

3.5. Final updated land cover map 2015

The final land cover map for 2015 is composed of the original 2013 land cover labels for the pixels designated as unchanged in the binary change map. The pixels that are designated as changed take the label from the 2015 IVM classification, as do the areas covered by cloud or cloud shadow in 2013. As many IVM classifications were carried out for 2015, the one with the highest overall accuracy was used to update the labels. Cloud cover from 2015 was masked in the final map so that no out-of-date land class labels remain. The accuracy of this final land cover map for 2015 was tested using the same test data set as for the 2015 classification.

Table 3
Test data used for the various 2015 land cover classifications.

	Number of test points
Forest	741
Pasture	700
Secondary veg.	319
Urban	252
Water	302
Total	2314

3.6. Land cover change 2013–2015

Finally, we compare the land cover map for 2013 with the final updated land cover map for 2015 to identify areas of deforestation. We compare the results to the PRODES dataset for deforestation in 2014 and 2015 (INPE, 2016).

4. Results

4.1. Land cover classification 2013

The 2013 classification results provide the starting point for the rest of the SCD-SC method. The resulting 2013 land cover map for the study site is shown in Fig. 4. Unsurprisingly, forest dominates the study site, with 19,244 km^2 covered by this land cover type, 66.3% of the study area. Secondary vegetation covers 5632 km^2 (19.4%), pasture 3005 km^2 (10.4%), urban 1023 km^2 (3.5%) and water 124 km^2 (0.4%).

There is a distinct pattern for pasture in the study site, following the BR-163 highway and branching out on both sides. The main rivers in the study region have also been picked out by the classification, as well as some other water bodies (Fig. 4B). The urban area of Novo Progresso can be seen towards the centre of the map, and there are some much smaller urban settlements along the BR-163. However, these urban areas are hard to distinguish from other large areas classified as urban along the BR-163 highway, which do not correspond to real settlements or impervious surfaces. In addition, the areas classified as urban which are far away from the highway, often in the middle of pasture (Fig. 4B), are incorrectly classified.

The map shows secondary vegetation around the edges of pasture (Fig. 4A), which is consistent with the findings of Müller et al. (2016b). Secondary vegetation can also be seen as a salt and pepper effect within primary forest, a minority of which represents outcrops of hilly terrain close to Novo Progresso with variable density of vegetation cover. Secondary vegetation is also present as distinct geometrical patches, presumably in areas that are recovering after deforestation.

The overall accuracy of the 2013 classification is 82.5%. The confusion matrix shows that there is significant confusion between secondary vegetation and forest, and secondary vegetation and pasture (Table 4). This caused a relatively low user’s accuracy for secondary vegetation (53%) and contributed to the producer’s accuracies observed for forest and pasture.

More surprisingly, there is also significant confusion between the classes urban and pasture, reflected in the user’s accuracy for urban of 73.1%. This is likely to be due to the difficulty in finding pixels where the dominant land cover is man-made, impermeable surfaces, because in Novo Progresso the urban areas contain a variety of land covers including impervious surfaces, bare soil and vegetation, with different parts of urban settlements containing different proportions of each. This likely led to a mixed pixel problem, causing spectral similarity between urban and other classes (such as pasture), as well as a large amount of spectral variation between pixels labelled as urban.

4.2. Spectral change detection 2013–2015

The results of the RCVMAX analysis between 2013 and 2015 show a pattern of high spectral change similar to the pattern of non-forest areas (Fig. 5B). The per-class a_j values to determine the threshold of how much spectral change can occur before land cover change was declared were set at 0.25 for forest and secondary vegetation, 0.5 for pasture and urban, and 1.5 for water. This is consistent with the fact that forests typically maintain relatively stable spectral signatures over many years, while most other non-forest land cover types have more spectral variability (Huang et al., 2010).

The resulting binary change map, after the thresholds were applied,

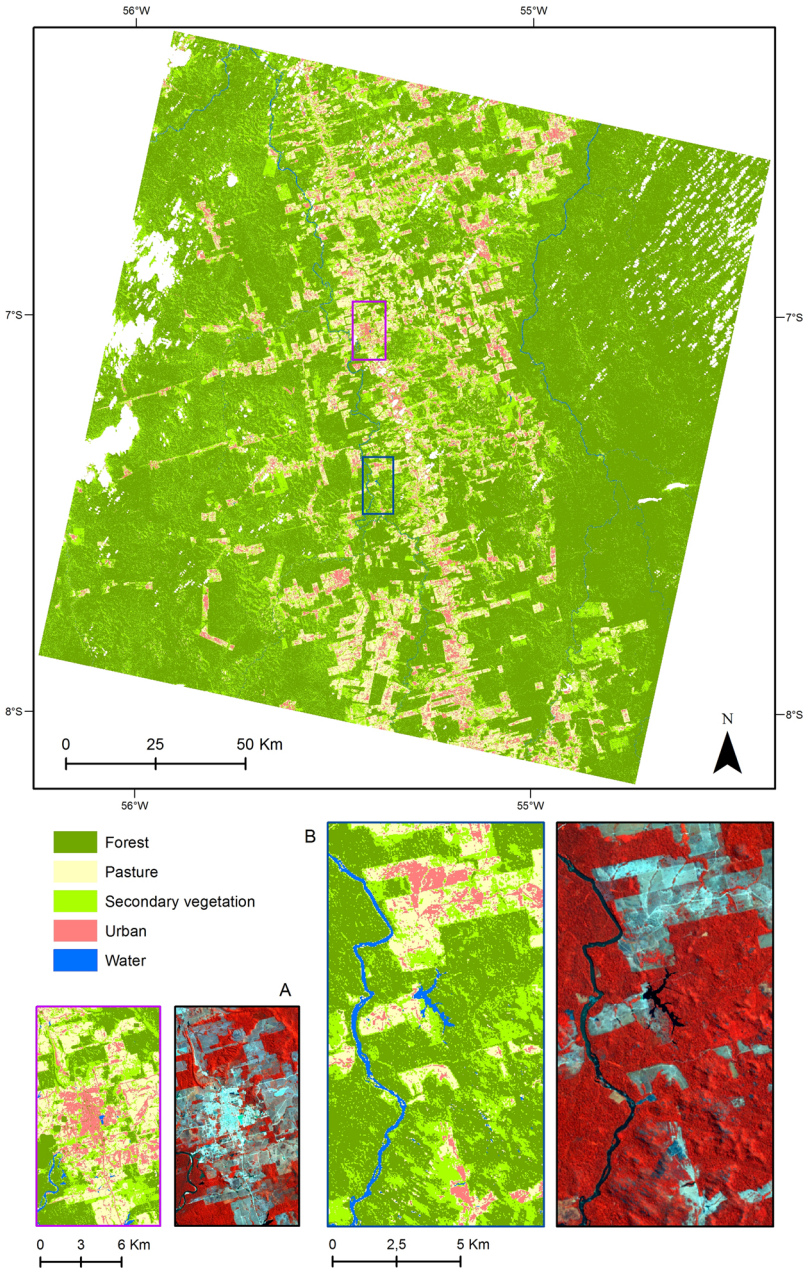

Fig. 4. Land cover map of the study site for 2013, based on the IVM classification using Landsat scenes for the day of year (DOY) 236 2013 and DOY 172 2013. Clouds are masked for both dates. The subsets of the map A and B compare land cover to Landsat 2013 236 (bands NIR, Green and Blue). (For interpretation of the references to colour in this figure legend, the reader is referred to the web version of this article.)

is displayed in Fig. 5A and identifies 1891 km^2 of potential change between 2013 and 2015, representing about 6% of the scene. The most change is mapped for the class forest (705 km^2), followed by secondary vegetation (650 km^2), pasture (383 km^2), urban (151 km^2) and only 2 km^2 for water.

A visual assessment of the binary change map shows that the areas around some of the clouds have been identified as changed, due to spectral change where no land cover change occurred. A closer inspection confirms that change has often been over-estimated (Fig. 5B). However, a large area still remains mapped as unchanged which can be sampled for training data in the following step.

The accuracy assessment of the change map confirms this assessment and shows that of the 95 samples from the change stratum, 55 were considered to have no real land cover change during the period 2013–2015. All of the 218 samples drawn from the no-change stratum were identified as no land cover change, so there is no omission error for change. This confirms that the thresholds for bi-temporal change detection were set in a way that minimises the error of omission for the change area, ensuring that pixels that change between the dates do not go on to form part of the training pool for the 2015 classification and are instead reclassified.

4.3. Land cover classification 2015

The land cover classification for 2015 was performed in two different ways, using (i) randomly selected training samples and (ii) training samples with high classification probabilities. For each of the two approaches the number of training samples was varied. As expected, the classification accuracy usually increases with an increasing number of training samples. When the training samples are taken randomly from the unchanged area the mean overall accuracy increases steadily, until it reaches 72.2 (± 1.5)% when 1000 points are used,

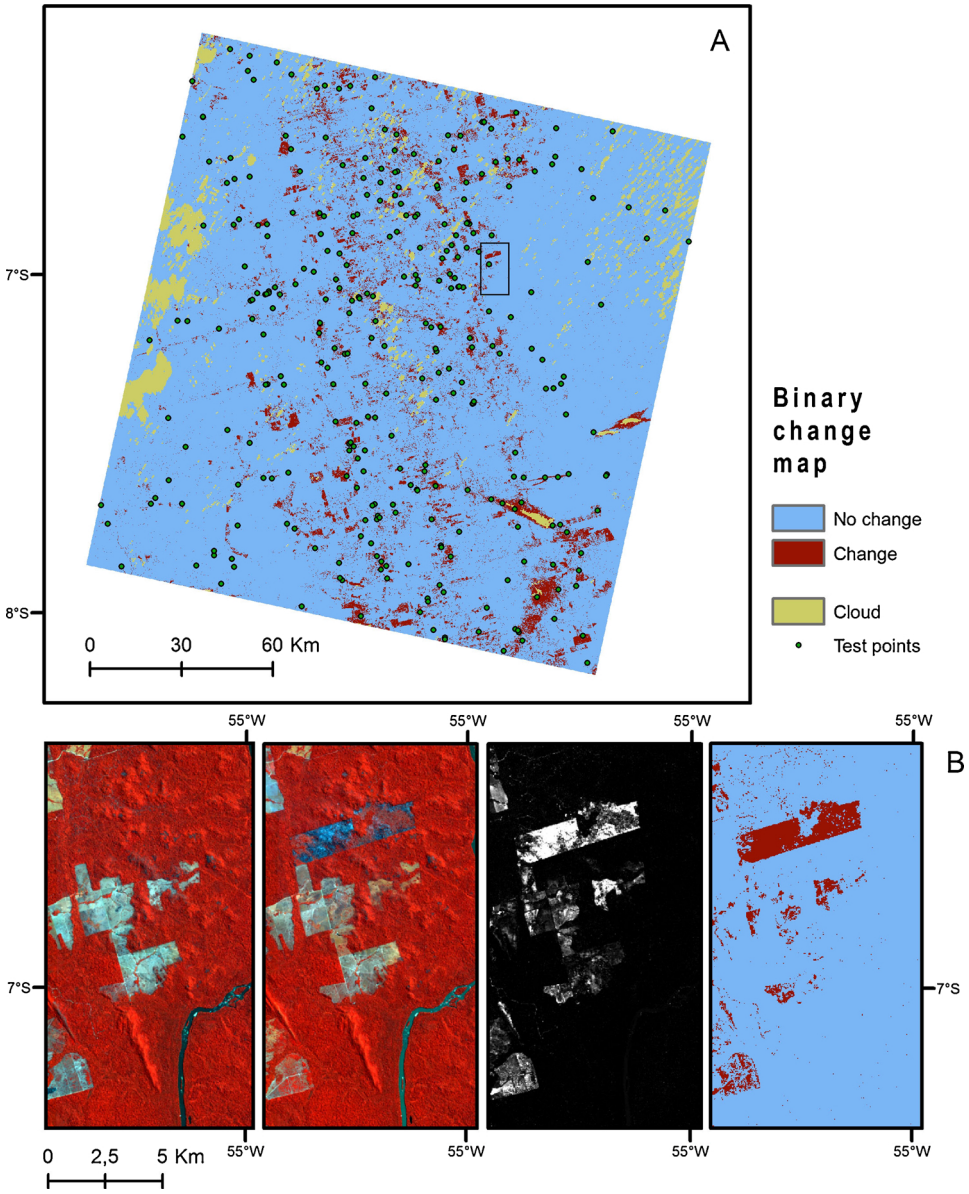

Fig. 5. Binary change map (A), based on Landsat scenes DOY 236 2013 and 226 2015, but masked with the clouds from all four dates. The change detection procedure is demonstrated in B for a subset of the map, the extent of which is indicated in map A. The subset shows (from left to right) the early Landsat scene, the late Landsat scene, RCVMAX derived from this pair of Landsat images and the binary change map after thresholds have been applied.

Table 4
Confusion matrix, overall accuracy, producer's accuracies, user's accuracies and kappa value for the 2013 classification.

		Map					Correct	Total	PA[a] (%)
		Forest	*Pasture*	*Sec. veg.*	*Urban*	*Water*			
Reference	Forest	**545**	3	121	0	0	545	669	81.5
	Pasture	2	**415**	50	65	1	415	533	77.9
	Sec. veg.	56	11	**194**	0	0	194	261	74.3
	Urban	0	11	0	**177**	0	177	188	94.1
	Water	0	3	0	0	**196**	196	199	98.5
Correct		545	415	194	177	196	**1527**		
Total		603	443	365	242	197		**1850**	
UA[b] (%)		90.4	93.7	53.2	73.1	99.5	**Overall accuracy: 82.5%**		
							Kappa: 0.77		

[a] PA – producer's accuracy.
[b] UA – user's accuracy.

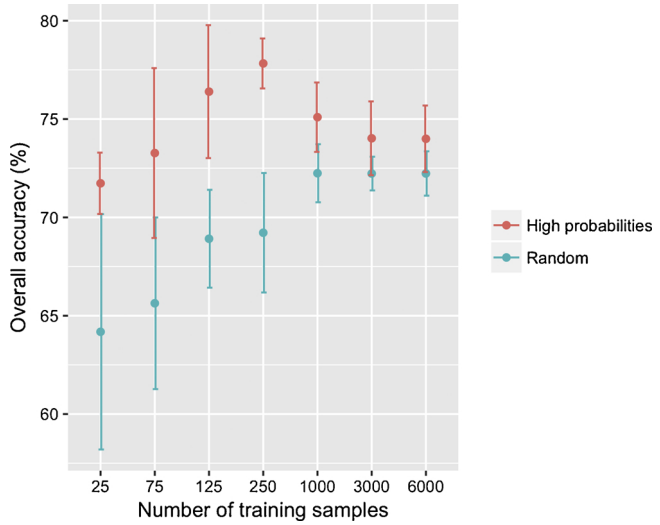

Fig. 6. Mean and standard deviation of overall accuracy for various 2015 classifications, using training samples of different sizes. For each training sample size 10 classifications were run using the pixels with high classification probabilities, and 10 classifications were run with different sets of randomly selected pixels.

after which it levels out and even drops off slightly. When the training samples with high probabilities are used the mean overall accuracy peaks at 77.8 (± 1.3)%, when 250 training samples are used. When more than 250 points are used the mean overall accuracy drops quickly (Fig. 6).

The use of probabilities in the selection of training samples significantly improves the results compared to a random selection when 250 training samples or less are used. However, when a very large number of training samples is considered (1000 or more), the two selection strategies show no significant difference in overall accuracy.

The results of two classifications are presented here in more detail, representing the two approaches to training data selection and taken from the runs with the highest mean overall accuracy in each case. Thus, the classification with the highest overall accuracy was taken from the run using 1000 randomly selected training points (overall accuracy 74.0%) and from the run using 250 training points with high probabilities (overall accuracy 79.4%) (Fig. 7). The McNemar statistical test indicates that the classification using 250 training points with high probabilities resulted in a significantly more accurate map ($p < 0.001$) compared to the classification using 1000 randomly selected training points (The value for $|z|$ was 104.1).

Visually, the most striking difference between the two different approaches is that Fig. 7A, created based on training samples randomly selected from the unchanged area, has a much larger area mapped as urban. This map classifies 1714 km^2 as urban, about 5.7% of the scene. The vast majority of this area is not in fact built up areas, and urban has a user's accuracy of 48.0% (Table 5). A total of 18,132 km^2 were mapped as primary forest (60.1%) in this classification, 3542 km^2 as pasture (11.7%), 6596 km^2 as secondary vegetation (21.8%) and 203 km^2 as water (0.7%).

For the map created using training samples with high classification probabilities (Fig. 7B), only 741 km^2 (2.5%) of the study area is mapped as urban. A comparatively small area has been mapped as primary forest (17,398 km^2, 57.6%) and larger areas are mapped as pasture (4430 km^2, 14.7%) and secondary vegetation (7513 km^2, 24.9%). The misclassification of forest as pasture and secondary vegetation is also evident from the confusion matrix and the lower producer's accuracy for forest (Table 6). The class water covers 104 km^2 (0.3%) of the study area.

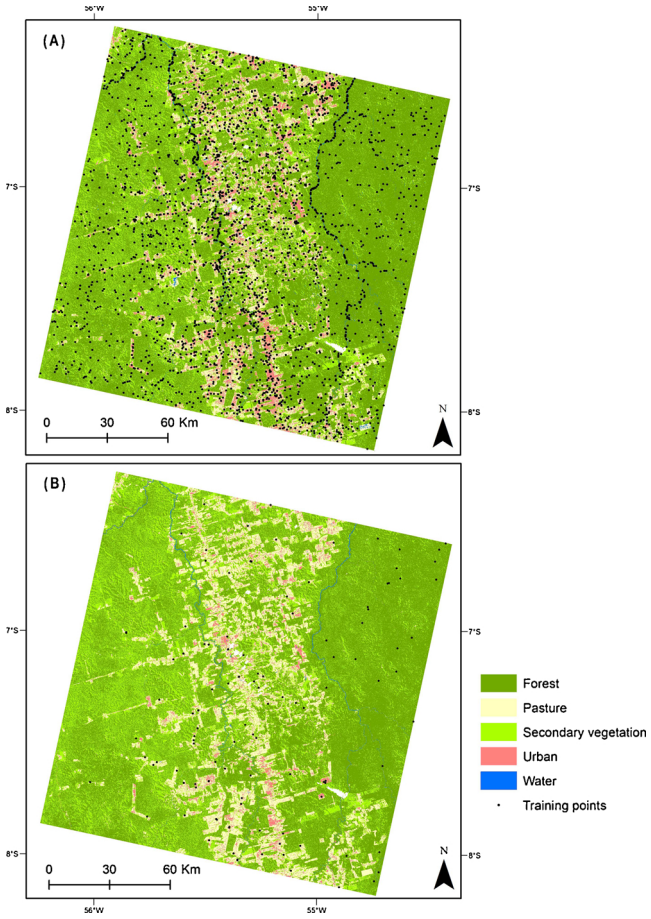

Fig. 7. Land cover map for 2015. (A) is based on randomly selected training samples; (B) is based on training samples with high classification probabilities.

4.4. Final updated land cover for 2015

The final composite map for 2015, updated from 2013, can be seen in Fig. 8. It is based on the land cover map for 2013. The areas detected as changed between 2013 and 2015 have been updated using the 2015 land cover map with the highest classification accuracy, achieved using 250 training samples with high classification probabilities (see also Fig. 7B).

The overall accuracy for this updated map is 80.1%. Similar to the previous classifications, secondary vegetation is challenging to map accurately, resulting in relatively low producer's and user's accuracies (Table 7). Visually the final updated map for 2015 is very similar to the original 2013 land cover map, as would be expected given the method behind the creation of the map, as well as the relatively small time gap between the land cover maps. Forest covers 19,516 km^2 (64.7% of the scene), pasture 3616 km^2 (12%), secondary vegetation 5795 km^2 (19.2%), urban 1133 km^2 (3.7%) and water 128 km^2 (0.4%).

4.5. Land cover change 2013–2015

When the updated land cover map for 2015 is compared with the 2013 land cover map the pattern of loss of primary forest is very similar to that of the PRODES data set, as can be seen in the map subsets in Fig. 9. The total loss of primary forest between the two dates is 447 km^2, amounting to 1.5% of the scene. This is mostly in the form of discrete quadratic areas, occurring up to 65 km away from the BR-163 highway.

Table 5
Confusion matrix, overall accuracy, producer's accuracies, user's accuracies and kappa value for a 2015 classification using randomly selected training points.

		Map					Correct	Total	PA[a] (%)
		Forest	*Pasture*	*Sec. veg.*	*Urban*	*Water*			
Reference	Forest	**604**	3	132	0	2	604	741	81.5
	Pasture	2	**313**	114	269	2	313	700	44.7
	Sec. veg.	57	10	**246**	1	5	246	319	77.1
	Urban	0	1	0	**251**	0	251	252	99.6
	Water	0	1	0	2	**299**	299	302	99.0
Correct		604	313	246	251	299	**1713**		
Total		663	328	492	523	308		**2314**	
UA[b] (%)		91.1	95.4	50.0	48.0	97.1	**Overall accuracy: 74.0%** Kappa: 0.67		

[a] PA – producer's accuracy.
[b] UA – user's accuracy.

5. Discussion

We proposed an approach to map land cover change in the Brazilian Amazon using a spectral change detection-supervised classification (SCD-SC) method. As the supervised classification demands an (automatic) selection of adequate training samples in unchanged areas, the first objective of this study was to explore the potential of using classification probabilities as criteria for training sample selection within the SCD-SC method. This was found to increase the overall accuracy of the 2015 classifications, although when 1000 training samples or more were used the increase in accuracy was not significant.

However, it is worth highlighting that using even a small number of training samples with high probabilities results in high classification accuracies, e.g.: The best overall accuracy for 2015 was 77.8%, achieved when probabilities were used as additional selection criteria and only 250 training samples were used (50 training samples per class). Within this approach the mean overall accuracy dropped when more than 250 samples were used, presumably because pixels with lower classification probabilities were introduced, which were more likely to be incorrectly labelled.

Selecting training samples at random results in significantly lower classification accuracies for small sample sets. As the size of the trainings samples increases, the resulting accuracy also goes up, as would be expected. However, these accuracies are still below the respective results achieved when classification probabilities were used as additional selection criteria, even for very large sample sizes. One reason for this might be that selecting a very high number of training samples results in the selection of inadequate, i.e. mislabelled training samples, particularly for small classes and those more difficult to classify.

It is significant that a better result was achieved with fewer training samples when probabilities were used as additional training criteria, as it means that this approach has the additional advantage of reducing computation time. The IVM classifications took approximately 5 min when 250 training samples were used and approximately 20 min when 1000 training samples were used. This is particularly relevant when a large area needs to be mapped or an update needs to be completed quickly.

Other approaches could be used to acquire training samples for the later date, including masking the existing training data set through the change detection process (Schulte to Bühne et al., 2017). No work was carried out here to assess this option, but the benefits of selecting training samples from the unchanged area include the ability to (i) easily increase the number of training samples if necessary; (ii) standardise the method of training sample selection when the method is applied over large areas with different numbers and qualities of training samples originally; and (iii) the possibility of updating an existing land cover map by somebody who does not have access to the original training data set, provided that they have access to the scenes used to create the map and a georeferenced land cover raster (including associated probabilities if these are to be used in training data selection).

The second objective of this study was to assess the suitability of the modified SCD-SC method for use in a tropical forest system. Xian et al. (2009) show that the SCD-SC method works well for various ecoregions across the USA experiencing different types of land cover change, including wildland fire and urban expansion. However, tropical forest systems generally, and the Amazon in particular, offer a series of specific challenges to the application of the method. The Amazon rainforest experiences rapid land use change, in particular forest clearance, and slash and burn practices in pastures, followed by comparatively quick re-growth of secondary vegetation during extended fallow periods or shifting cultivation (Fearnside, 2000). Together this leads to cycles of deforestation and recovery, with secondary vegetation sometimes

Table 6
Confusion matrix, overall accuracy, producer's accuracies, user's accuracies and kappa value for a 2015 classification using training points with high classification probabilities.

		Map					Correct	Total	PA[a] (%)
		Forest	*Pasture*	*Sec. veg.*	*Urban*	*Water*			
Reference	Forest	**572**	4	165	0	0	572	741	77.2
	Pasture	2	**465**	116	117	0	465	700	66.4
	Sec. veg.	46	8	**259**	1	5	259	319	81.2
	Urban	0	4	0	**248**	0	248	252	98.4
	Water	0	7	0	2	**293**	293	302	97.0
Correct		572	465	259	248	293	**1837**		
Total		620	488	540	368	298		**2314**	
UA[b] (%)		92.3	95.3	48.0	67.4	98.3	**Overall accuracy: 79.4%** Kappa: 0.74		

[a] PA – producer's accuracy.
[b] UA – user's accuracy.

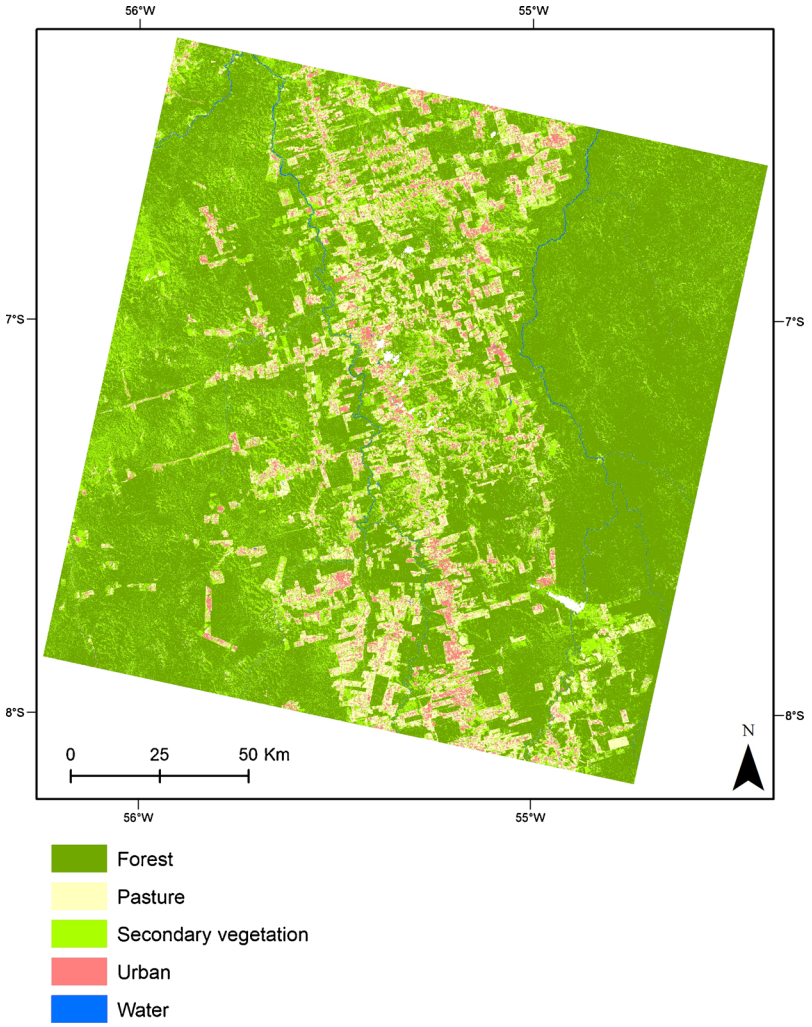

Fig. 8. Final updated map for 2015, based on the land cover map for 2013, with land cover labels taken from the 2015 classification in areas detected as changed in the binary change map. Clouds have been masked for 2015.

Table 7
Confusion matrix and accuracies for the final updated land cover map for 2015.

		Map					Correct	Total	PA[a] (%)
		Forest	*Pasture*	*Sec. veg.*	*Urban*	*Water*			
Reference	Forest	**647**	3	90	1	0	647	741	91.9
	Pasture	13	**413**	123	151	0	413	700	93.0
	Sec. veg.	40	21	**252**	1	5	252	319	54.2
	Urban	4	3	0	**245**	0	245	252	61.3
	Water	0	4	0	2	**296**	296	302	98.3
Correct		647	413	252	245	296	**1853**		
Total		704	444	465	400	301		**2314**	
UA[b] (%)		87.3	59.0	79.0	97.2	98.0	**Overall accuracy: 80.1%** Kappa: 0.74		

[a] PA – producer's accuracy.
[b] UA – user's accuracy.

repeatedly removed (Müller et al., 2016b). In order for the dynamics of these cycles of land cover change to be successfully mapped by the SCD-SC method, it needs to be able to distinguish between primary forest, secondary vegetation and pasture.

When the land cover maps for 2013 and 2015 were used to track the loss of primary forest, the pattern was found to be very similar to PRODES. In addition, the loss of about 447 km^2 of primary forest mapped between 2013 and 2015 in the 30,260 km^2 study region is similar to the 436 km^2 of deforestation reported by PRODES for a very similar time period, albeit for a slightly smaller area. This suggests that this modified SCD-SC method may be fit for purpose as long as the aim of the study is to map loss of primary forest, with no emphasis on the land cover it changes to.

The results show that the initial confusion between forest, secondary vegetation and pasture in the 2013 map was exacerbated during the update to 2015. This led to a drop in the overall accuracy from 82.5% for the 2013 classification to 80.1% for the final composite 2015 land cover map. This is likely to be, at least in part, because

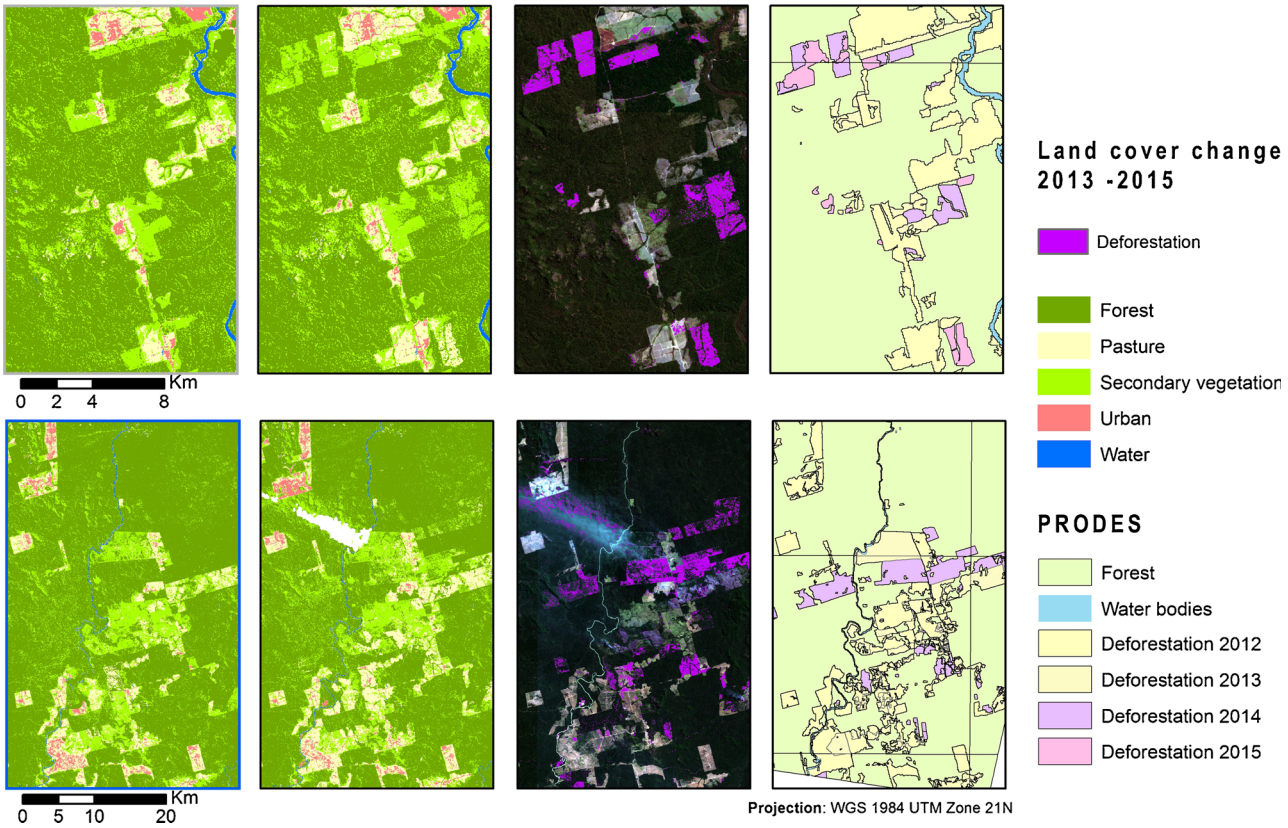

Fig. 9. Two map subsets show, from left to right, the land cover map for 2013, the final updated land cover map 2015, the map of deforestation (loss of primary forest) and the PRODES 2015 data set for the same area.

misclassified pixels were chosen to train the 2015 classification, despite the use of classification probabilities in the training sample selection process. Whilst this is not a general limitation of the approach – the confusion between forest, secondary vegetation and pasture could be reduced in the 2013 classification by integrating additional imagery – it does highlight the importance of an excellent starting map for the method. The SCD-SC method thus makes most sense when there is an excellent land cover map already in place, especially if time-consuming post-processing steps such as manual corrections or even manual mapping of less common classes have been carried out, as these will appear again on the updated composite map unless detected as changed. For example, given the misclassification of pasture as urban in our study, it may be that manually mapping urban areas is sensible, as was done in Almeida et al. (2016).

Given that much of the land cover change in the Amazon occurs quickly and sometimes cyclically, one strength of the SCD-SC is that it can potentially provide regular updates without the need to collect new training samples. Various trajectory-based change detection methods are also able to do this by using a dense temporal stack of optical images to detect forest disturbance and recovery (Kennedy et al., 2007; Huang et al., 2010) or land cover change for many classes (Zhu and Woodcock, 2014). However, these methods are usually computationally more complex, when compared to a simple SCD-SC method, and encounter similar difficulties in defining change. Moreover, these methods usually need dense time series and can have problems with overfitting if the data are always missing for a certain time of year because of clouds (Zhu and Woodcock, 2014). This might be a limitation for tropical Amazon regions, where cloud cover is very high during the wet season. In the case of the SCD-SC method, high cloud cover during the wet season does not have any detrimental effect on land cover mapping during the dry period, even if it limits land cover information to the dry season. In terms of repeatedly updating a land cover map using the SCD-SC method, more work needs to be done to ascertain if confusion between classes is exacerbated over time due to frequent updates.

An additional benefit to our approach is that the SCD-SC method enables the use of additional remote sensing imagery, e.g. Synthetic Aperture Radar (SAR) data. During the classification procedure SAR data are almost weather independent and might help overcome the spectral ambiguities of multispectral data. This would also be in accordance with the findings in Joshi et al. (2016) that identified the need for methods and applications to map broad land cover or land use classes, and the changes therein, using optical and SAR data.

6. Conclusion

We proposed an approach to map land cover change in the Brazilian Amazon, using spectral change detection and a supervised, probabilistic classifier. The classification probabilities were used as criteria for trainings data selection in areas identified as unchanged, representing the confidence in the class label. The results show that this use of classification probabilities proves useful in terms of accuracy and computational complexity. Compared to the classification using randomly selected training samples, the use of high classification probabilities increased overall accuracy and greatly reduced the number of training samples required, resulting in lower computation time.

The probabilistic SCD-SC method applied in this study shows potential to map the dynamic land cover change in the Amazon during the dry, low-cloud cover season, although some challenges remain. The efficiency of the SCD-SC, both in terms of speed of implementation, level of automation and computation power needed, has potential to map very large areas such as the Amazon rainforest. Beyond this, the ability to quickly update only parts of an existing, high quality map could also be relevant for other applications, such as in disaster management, where an up-to-date map is important to inform disaster response.

Acknowledgments

This study was partly funded by the research project SenseCarbon (FKZ, 50 EE 1255), funded by the German Space Agency (DLR) and the Federal Ministry for Economic Affairs and Energy (BMWi).

RapidEye data was provided by a RESA proposal (ID 704).

References

Agresti, A., 2002. Categorical Data Analysis. John Wiley and Sonshttps://doi.org/10.1198/tech.2003.s28.

Almeida, C.A., de Coutinho, A.C., Esquerdo, J.C.D.M., Adami, M., Venturieri, A., Diniz, C.G., Dessay, N., Durieux, L., Gomes, A.R., 2016. High spatial resolution land use and land cover mapping of the Brazilian Legal Amazon in 2008 using Landsat-5/TM and MODIS data. Acta Amazon. 46, 291–302.

Aragão, L.E.O.C., Malhi, Y., Barbier, N., Lima, A., Shimabukuro, Y., Anderson, L., Saatchi, S., 2008. Interactions between rainfall, deforestation and fires during recent years in the Brazilian Amazonia. Philos. Trans. R. Soc B: Biol. Sci. 363, 1779 LP–1785.

Asner, G.P., Townsend, A.R., Bustamante, M.M.C., Nardoto, G.B., Olander, L.P., 2004. Pasture degradation in the central Amazon: linking changes in carbon and nutrient cycling with remote sensing. Glob. Chang. Biol. 10, 844–862. https://doi.org/10.1111/j.1529-8817.2003.00766.x.

Belgiu, M., Drăguţ, L., 2016. Random forest in remote sensing: a review of applications and future directions. ISPRS J. Photogramm. Remote. Sens. 114, 24–31.

Betts, R.A., Cox, P.M., Collins, M., Harris, P.P., Huntingford, C., Jones, C.D., 2004. The role of ecosystem-atmosphere interactions in simulated Amazonian precipitation decrease and forest dieback under global climate warming. Theor. Appl. Climatol. 78, 157–175. https://doi.org/10.1007/s00704-004-0050-y.

Braun, A.C., Weidner, U., Hinz, S., 2012. Classification in high-dimensional feature spaces - assessment using SVM, IVM and RVM with focus on simulated EnMAP data. IEEE J. Sel. Top. Appl. Earth Obs. Remote. Sens. 5, 436–443. https://doi.org/10.1109/JSTARS.2012.2190266.

Congalton, R.G., Green, K., 2009. Assessing the Accuracy of Remotely Sensed Data: Principles and Practices, 2nd ed. CRC Press/Taylor & Francis, Boca Raton.

Coy, V.M., Klingler, M.M., 2011. Pionierfronten im brasilianischen Amazonien zwischen alten Problemen und neuen Dynamiken. Das Beispiel des “Entwicklungskorridors” Cuiabá (Mato Grosso)–Santarém (Pará). Innsbrucker Bericht 2008–2010.

DNPM, 1983. Projeto RADAMBRASIL, 1973–1983. Levantamento de Recursos Naturais, Fearnside.

Fearnside, P.M., 2000. Global warming and tropical land-use change: greenhouse gas emissions from biomass burning, decomposition and soils in forest conversion, shifting cultivation and secondary vegetation. Clim. Change 46, 115–158. https://doi.org/10.1023/A:1005569915357.

Foody, G.M., 2004. Thematic map comparison: evaluating the statistical significance of differences in classification accuracy. Photogramm. Eng. Remote Sensing 70 (5), 627–633.

Foody, G.M., Mathur, A., 2004. A relative evaluation of multiclass image classification of support vector machines. IEEE Trans. Geosci. Remote. Sens. 42, 1335–1343.

Fry, J.A., Coan, M.J., Homer, C.G., Meyer, D.K., Wickham, J.D., 2009. Completion of the National Land Cover Database (NLCD) 1992-2001 Land Cover Change Retrofit Product. U.S. Geological Survey Open-File Report 2008. pp. 1–18.

Fry, J.A., Xian, G., Jin, S., Dewitz, J.A., Homer, C.G., Yang, L., Barnes, C.A., Herold, N., Wickham, J.D., 2011. Completion of the 2006 national land cover database for the conterminous United States. Photogramm. Eng. Remote Sensing 77, 858–866.

Galvão, L.S., Ponzoni, F.J., Liesenberg, V., Santos, J.R., 2009. Possibilities of discriminating tropical secondary succession in Amazônia using hyperspectral and multiangular CHRIS/PROBA data. Int. J. Appl. Earth Obs. Geoinf. 11 (1), 8–14. https://doi.org/10.1016/j.jag.2008.04.001.

Hagensieker, R., Roscher, R., Rosentreter, J., Jakimow, B., 2017. Tropical Land Use Land Cover Mapping in Pará (Brazil) using discriminative markov random fields and multi-temporal TerraSAR-X data. Int. J. Appl. Earth Obs. Geoinf. 63, 244–256. https://doi.org/10.1016/j.jag.2017.07.019.

Homer, C.G., Dewitz, J.A., Yang, L., Jin, S., Danielson, P., Xian, G., Coulston, J., Herold, N.D., Wickham, J.D., Megown, K., 2015. Completion of the 2011 National Land Cover Database for the conterminous United States-representing a decade of land cover change information. Photogramm. Eng. Remote Sensing 81, 345–354. https://doi.org/10.14358/PERS.81.5.345.

Hooper, D.U., Adair, E.C., Cardinale, B.J., Byrnes, J.E.K., Hungate, B.A., Matulich, K.L., Gonzalez, A., Duffy, J.E., Gamfeldt, L., O/’Connor, M.I., 2012. A global synthesis reveals biodiversity loss as a major driver of ecosystem change. Nature 486, 105–108.

Huang, C., Goward, S.N., Masek, J.G., Thomas, N., Zhu, Z., Vogelmann, J.E., 2010. An automated approach for reconstructing recent forest disturbance history using dense Landsat time series stacks. Remote Sens. Environ. 114, 183–198. https://doi.org/10.1016/j.rse.2009.08.017.

INPE, 2016. Projeto PRODES, Monitoramento da Floresta Amazônica Brasileira por Satélite. URL. (Accessed 11 November 2015). http://www.obt.inpe.br/prodes/.

Jakimow, B., Griffiths, P., van der Linden, S., Hostert, P., 2018. Mapping pasture management in the Brazilian Amazon from dense Landsat time series. Remote Sens. Environ. 205, 453–468. https://doi.org/10.1016/J.RSE.2017.10.009.

Jin, S., Yang, L., Danielson, P., Homer, C., Fry, J., Xian, G., 2013. A comprehensive change detection method for updating the National Land Cover Database to circa 2011. Remote Sens. Environ. 132, 159–175. https://doi.org/10.1016/j.rse.2013.01.012.

Joshi, N., Baumann, M., Ehammer, A., Fensholt, R., Grogan, K., Hostert, P., Jepsen, M.R., Kuemmerle, T., Meyfroidt, P., Mitchard, E.T.A., Reiche, J., Ryan, C.M., Waske, B., 2016. A review of the application of optical and radar remote sensing data fusion to land use mapping and monitoring. Remote Sens. 8 (1), 1–23.

Kennedy, R.E., Cohen, W.B., Schroeder, T.A., 2007. Trajectory-based change detection for automated characterization of forest disturbance dynamics. Remote Sens. Environ. 110, 370–386. https://doi.org/10.1016/j.rse.2007.03.010.

Kintisch, E., 2015. Amazon rainforest ability to soak up carbon dioxide is falling. Science. https://doi.org/10.1126/science.aab0336. March 18.

Lapola, D.M., Martinelli, L.A., Peres, C.A., Ometto, J.P.H.B., Ferreira, M.E., Nobre, C.A., Aguiar, A.P.D., Bustamante, M.M.C., Cardoso, M.F., Costa, M.H., Joly, C.A., Leite, C.C., Moutinho, P., Sampaio, G., Strassburg, B.B.N., Vieira, I.C.G., 2014. Pervasive transition of the Brazilian land-use system. Nat. Clim. Change 4, 27–35.

Lu, D., Mausel, P., Brondizio, E., Moran, E., 2004. Change detection techniques. Int. J. Remote Sens. 25, 2365–2407. https://doi.org/10.1080/0143116031000139863.

Morisette, J.T., Khorram, S., 2000. Accuracy assessment curves for satellite-based change detection. Photogramm. Eng. Remote Sensing 66, 875–880.

Mountrakis, G., Im, J., Ogole, C., 2010. Support vector machines in remote sensing: a review. ISPRS J. Photogramm. Remote. Sens. 66 (3), 247–259.

Müller, H., Griffiths, P., Hostert, P., 2016a. Long-term deforestation dynamics in the Brazilian Amazon – uncovering historic frontier development along the Cuiabá – Santarém highway. Int. J. Appl. Earth Observ. Geoinf. 44, 61–69. https://doi.org/10.1016/j.jag.2015.07.005.

Müller, H., Rufin, P., Griffiths, P., de Barros, Viana, Hissa, L., Hostert, P., 2016b. Beyond deforestation: differences in long-term regrowth dynamics across land use regimes in southern Amazonia. Remote Sens. Environ. 186, 652–662. https://doi.org/10.1016/j.rse.2016.09.012.

Nobre, A.D., 2014. The Future Climate of Amazonia. Scientific Assessment Report, Sao José Dos Campos.

Pan, Y., Birdsey, R.A., Fang, J., Houghton, R., Kauppi, P.E., Kurz, W.A., Phillips, O.L., Shvidenko, A., Lewis, S.L., Canadell, J.G., Ciais, P., Jackson, R.B., Pacala, S.W., McGuire, A.D., Piao, S., Rautiainen, A., Sitch, S., Hayes, D., 2011. A large and persistent carbon sink in the world’s forests. Science 333, 988 LP–993.

Roscher, R., 2014. Import Vector Machine Classifier version 4.4.

Roscher, R., Förstner, W., Waske, B., 2012a. I 2VM: incremental import vector machines. Image Vis. Comput. 30, 263–278. https://doi.org/10.1016/j.imavis.2012.04.004.

Roscher, R., Waske, B., Förstner, W., 2012b. Incremental import vector machines for classifying hyperspectral data. IEEE Trans. Geosci. Remote. Sens. 50, 3463–3473. https://doi.org/10.1109/TGRS.2012.2184292.

Rosentreter, J., Hagensieker, R., Okujeni, A., Roscher, R., Wagner, P.D., Waske, B., 2017. Subpixel mapping of urban areas using EnMAP data and multioutput support vector regression. IEEE J. Sel. Top. Appl. Earth Obs. Remote. Sens. 1–11.

Rufin, P., Müller, H., Pflugmacher, D., Hostert, P., 2015. Land use intensity trajectories on Amazonian pastures derived from Landsat time series. Int. J. Appl. Earth Obs. Geoinf. 41, 1–10. https://doi.org/10.1016/j.jag.2015.04.010.

Schulte to Bühne, H., Wegmann, M., Durant, S.M., Ransom, C., de Ornellas, P., Grange, S., Beatty, H., Pettorelli, N., 2017. Protection status and national socio-economic context shape land conversion in and around a key transboundary protected area complex in West Africa. Remote Sens. Ecol. Conserv. 3 (4), 190–201. https://doi.org/10.1002/rse2.47.

Suess, S., van der Linden, S., Leitao, P.J., Okujeni, A., Waske, B., Hostert, P., 2014. Import vector machines for quantitative analysis of hyperspectral data. IEEE Geosci. Remote. Sens. Lett. 11 (2), 449–453. https://doi.org/10.1109/Lgrs.2013.2265102.

Swann, A.L.S., Longo, M., Knox, R.G., Lee, E., Moorcroft, P.R., 2015. Future deforestation in the Amazon and consequences for South American climate. Agric. For. Meteorol. 214–215, 12–24. https://doi.org/10.1016/j.agrformet.2015.07.006.

USGS, 2016. Product Guide: Provisional Landsat 8 Surface Reflectance Product Guide. https://doi.org/10.1080/1073161X.1994.10467258.

Waske, B., van der Linden, S., 2008. Classifying multilevel imagery from SAR and optical sensors by decision fusion. IEEE Trans. Geosci. Remote Sens. 46 (5), 1457–1466.

Waske, B., Linden, S., Van Der Benediktsson, J.A., Rabe, A., Hostert, P., 2010. Sensitivity of support vector machines to random feature selection in classification of hyperspectral data. IEEE Trans. Geosci. Remote. Sens. 48, 2880–2889. https://doi.org/10.1109/TGRS.2010.2041784.

Werth, D., Avissar, R., 2002. The local and global effects of Amazon deforestation. J. Geophys. Res. 107https://doi.org/10.1029/2001JD000717. LBA 55-1–LBA 55-8.

Xian, G., Homer, C., Fry, J., 2009. Updating the 2001 National Land Cover Database land cover classification to 2006 by using Landsat imagery change detection methods. Remote Sens. Environ. 113, 1133–1147. https://doi.org/10.1016/j.rse.2009.02.004.

Zhu, J., Hastie, T., 2005. Kernel logistic regression and the import vector machine. J. Comput. Graph. Stat. 14, 185–205. https://doi.org/10.1198/106186005X25619.

Zhu, Z., Woodcock, C.E., 2014. Continuous change detection and classification of land cover using all available Landsat data. Remote Sens. Environ. 144, 152–171. https://doi.org/10.1016/j.rse.2014.01.011.

Zhu, Z., Woodcock, C.E., Rogan, J., Kellndorfer, J., 2012. Assessment of spectral, polarimetric, temporal, and spatial dimensions for urban and peri-urban land cover classification using Landsat and SAR data. Remote Sens. Environ. 117, 72–82.